Use of Ar-He mixed gas plasmas for furnace atomization plasma ionization mass spectrometry (FAPIMS)

Stewart, I. I.; Sturgeon, R.

Publisher's version / Version de l'éditeur:
https://doi.org/10.1039/b002204g
Journal of Analytical Atomic Spectrometry, 15, 9, pp. 1223-1232, 2000

JAAS
Full Paper

Use of Ar–He mixed gas plasmas for furnace atomisation plasma ionisation mass spectrometry (FAPIMS)†

Ian I. Stewart* and Ralph E. Sturgeon

Institute for National Measurement Standards, National Research Council of Canada, Building M12, Montreal Road Campus, Ottawa, Ontario, Canada K1A 0R6.
E-mail: ian.stewart@nrc.ca

Received 23rd March 2000, Accepted 27th June 2000
Published on the Web 24th August 2000

The effect of Ar–He mixed gas plasmas on analyte signal intensities generated in a furnace atomization plasma ionization mass spectrometry (FAPIMS) source is presented. Analyte is introduced as a volatile headspace gas effluent ($I_{2(g)}$ and $Hg_{(g)}$) and in discrete liquid sample volumes (Fe, Rb, Pd, In, Cs, Yb, Pt, Pb and Bi). The presence of as little as 2–10% (v/v) Ar increases the signal intensity of analytes having first ionization potentials greater than 6 eV by up to 10-fold. This may be attributed to the formation of more energetic plasmas whose electron density, ionization temperature and gas kinetic temperatures increase with Ar content. Consistent with this, elements with the highest ionization potentials showed the greatest enhancements. Analytes with ionization potentials of less than 6 eV, which are already presumed 100% ionized, are unaffected. Further increases in Ar content (50–100% v/v) can lead to plasma instability and accelerated erosion of graphite surfaces within the source. Most of the analytes studied showed slight improvements in the limits of detection for plasmas containing $\approx$5% v/v Ar; the increased signal intensity was accompanied by little or no increase in the background signal. Although Ar can significantly affect conditions within the source, the composition of the Ar–He mixture can also influence the transmission of analyte into the free jet expansion and to the MS detector. The appearance and intensity of Ar-based spectral interferences, such as ArC^+, ArO^+ and Ar_2^+, increase with Ar content and source temperature, degrading the determination of species such as $^{52}Cr^+$, $^{56}Fe^+$ and $^{80}Se^+$. The amount of Ar required to generate significant signal enhancements is small (<10% v/v) and therefore does not significantly ease the pumping requirements on the interface.

Introduction

Furnace atomization plasma ionization mass spectrometry (FAPIMS) is a relatively new technique that has demonstrated great potential for trace element analysis.[1,2] In FAPIMS, a small sample volume (*e.g.*, 2–10 μL) is injected through a dosing port into a transversely heated, integrated contact cuvette (ICC) graphite tube furnace.[3,4] Application of a suitable furnace program serves to vaporize/atomize sample directly into a capacitively coupled He plasma formed between an axial graphite rod electrode and the grounded wall of the ICC furnace (*i.e.*, within the annular volume of the furnace). The analyte is ionized in the plasma and rapidly sampled into the mass spectrometer through a two-stage sampler/skimmer interface. A significant advantage of this source design is that analyte is transported into the MS, thereby avoiding transport losses due to analyte deposition between the vaporiser and plasma normally associated with other coupled sources such as ETV-ICPMS.[5] The current FAPIMS sampling configuration provides a precision of $\approx$5%, linear dynamic range of 3–4 orders of magnitude and estimated absolute limits of detection of 20–500 fg for Mg, Fe, Co, Cu, Se, Cd, Cs and Pb.[2]

The use of He plasmas as an ion source has already been demonstrated for FAPIMS.[1,2,6] In addition to being readily initiated and easily sustained, He plasmas offer several potential advantages over their Ar counterparts.[7] These include a limited number of possible spectral interferences due to the near mono-isotopic abundance (99.999%) and low mass (4 amu) of He. Also, the high ionisation energy (24.48 eV) and the presence of a number of energetic species (such as He^+, He_2^+, He_m^*) augment the detection capability of difficult to ionise elements. Despite such advantages,[2] further optimisation and development of the source are necessary to provide the general robustness required for use with real samples. It is anticipated that such improvements would be relevant to analogous atmospheric pressure He rf plasma sources used for the MS detection of atomic and molecular ions in gas effluents.[8]

One promising new approach to improving the overall sensitivity and capability of the FAPIMS source is through the use of Ar–He mixed gas plasmas. Sun and Sturgeon[9,10] have demonstrated that emission intensities for a number of atom and ion lines are significantly enhanced when Ar–He plasmas are sustained within the FAPES source. Changing the gas composition from a pure He plasma to a pure Ar plasma increases the analyte ionization temperature (5270 to 6740 K), electron number density (*i.e.*, He 8×10^{13} cm^{-3}, Ar 1×10^{15} cm^{-3}) and gas kinetic temperature, thereby generating a more '*energetic*' plasma.[9] As such, the degree of ionization for elements having ionization potentials below 8 eV has been calculated to increase from >50% in pure He plasmas to >70% in argon plasmas in a FAPES source operated at 50 W.[9] Although the exact mechanism responsible for the increased ionization efficiency is unknown, it is certainly consistent with the formation of more energetic plasma conditions. In addition, specific Penning and charge transfer reactions between analyte and energetic argon species may be important for some elements.[9,10] In the FAPES source, however, increased analyte sensitivity did not lead to improved limits of detection (LODs) due to increased spectral interference from molecular background species.[10] Although direct spectral interferences may still occur with MS detection, the number of broad spectral overlaps from background species observed in FAPES[11–13] should be less severe in FAPIMS. The use of He-Ar mixed gas plasmas in the FAPIMS source, therefore,

†Presented at the 2000 Winter Conference on Plasma Spectrochemistry, Fort Lauderdale, FL, USA, January 10–15, 2000.

presents a potentially attractive means of improving the ionization efficiency and sensitivity for a wide range of elements, especially those for which the first ionization potentials are $\geqslant 8$ eV.

In this study, the influence of Ar–He mixed gas plasmas in a FAPIMS source are discussed in terms of improved analyte signal intensities, signal precision and LODs for both discrete sample volume (mass) introduction and for the steady-state introduction of gaseous Hg and I_2. A list of all the analytes and some of their important physical properties is given in Table 1. Significant features related to the composition of the gas mixture, such as vacuum requirements, analyte transport from the source to the MS detector, changes in the spectral background, polyatomic species formation and metal oxide levels, will also be considered.

Experimental

Apparatus

The FAPIMS source has been described in an earlier publication[2] and only a brief description will be given here. A 1 mm diameter graphite rod electrode (SGL Carbon, Ringsdorff-Werke GmbH, Germany) mounted in a brass collette serves as the powered rf electrode and coaxially traverses the length of a pyrolytic graphite coated ICC (SGL Carbon). The electrode terminates 1 mm from the end of the ICC tube facing the MS sampling interface (5–6 mm tube to sampling plate separation). The entire source is enclosed in a work-head fabricated from a copper block and fitted with ports for furnace power, purge gas, water cooling, rf power and optical temperature feedback (*cf.*, Fig. 1 from ref 2). The ICC furnace was heated by a Perkin-Elmer HGA-500 power supply and temperatures subsequently quoted are those read from the power supply, and may not reflect the true temperature of the ICC. Rf power (100 W) was supplied to the electrode from a Model RF10L 40 MHz generator and AM-5 matchbox (RF Power Products, Voorhees, NJ, USA). The work-head is mounted on the interface with three 1-inch micrometer heads, thereby permitting translation in three dimensions. The furnace was positioned so that the sampling orifice was on-line, but ≈ 1 mm below the central axis of the furnace (*i.e.*, 1 mm below the electrode and 2 mm above the bottom tube wall). This location permits sampling of a region of high plasma intensity,[17,18] yielding optimum signal intensity for most elements studied.[19]

A research prototype (test-bed) of a PE SCIEX Elan 6000 was used for all measurements. To handle the increased vacuum load due to He, a Varian SD-1400 (Varian Vacuum Products, Lexington, MA, USA) and a S25B (Leybold Canada Inc, Mississauga, Ontario, Canada) rotary pump having pumping speeds of 23.7 and 7.1 L s^{-1}, respectively, were connected to the interface. A Model PRM10 Pirani gauge with Model 503 controller (Edwards) was mounted about 15 cm from the interface to provide a continuous measure of the pressure in this region. The separation between the sampler (0.50 mm id) and skimmer (0.88 mm id) is ≈ 5.0 mm. Both sampler and skimmer cones sit on MACOR ceramic mounts, electrically isolated from the instrument ground. Voltages are applied to the sampler and skimmer cones using external dc power supplies (Hewlett-Packard, Models 6516A, and E3612A, respectively) and can be optimized for maximum signal intensity for each element. Because the FAPIMS source is low power (100 W) and the graphite furnace is operated intermittently (transient data collection) or at low relative temperatures (steady-state data collection), the interface was not water-cooled.

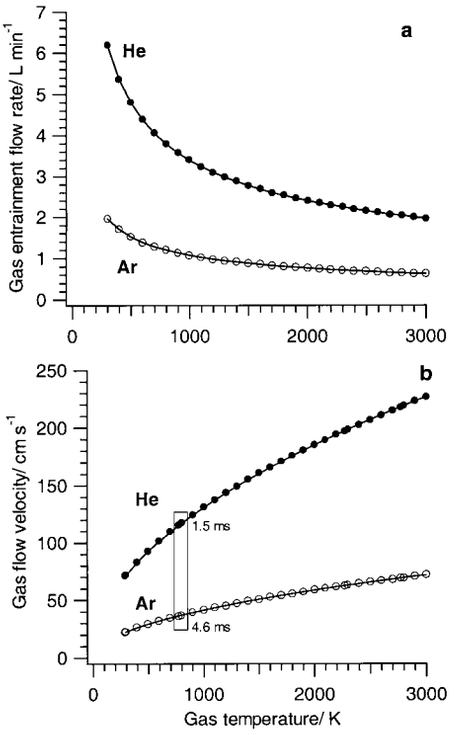

Fig. 1 Gas flow parameters for He and Ar as a function of temperature at atmospheric pressure. **a** Total gas flow rate through a 0.5 mm diameter sampling orifice. **b** The gas velocity calculated at a position 5 mm upstream from the sampling orifice, which coincides with the typical ICC tube position. Panel **b** inset shows the time required for each gas to travel from this position to the sampler at the given temperature.

Table 1 Physical properties of the selected analytes

Element	Isotopes monitored *m/z*	Volatility[a]	Ionization potential/eV[b]	
			I	II
Fe	56	Medium	7.87	16.18
Rb	85	Medium	4.18	17.05
In	113	High	5.79	20.29
Cs	133	Medium	3.89	21.50
Pd	106	Low (medium)	8.33	19.42
Yb	174	Low (medium)	6.20	12.10
Pt	195	Low (medium)	9.00	18.56
Pb	208	High (medium)	7.42	16.90
Bi	209	High (medium)	7.29	16.68
Hg	202	High	10.43	18.75
I_2	127[c], 254[d]	High	9.27[c], 10.45[d]	25.5[c], 19.13[d]

[a]Taken from ref. 14. [b]Taken from ref. 15. [c]Refers to I^+, taken from ref. 16. [d]Refers to I_2^+, taken from ref. 16.

Reagents

UHP grade He and Ar (Praxair, Ottawa, ON, Canada) were used for all experiments. Stock solutions (1000 mg^{-1}) of metals were prepared by dissolution of their nitrate or chloride salts in high purity deionized distilled water (DDW) obtained from a NanoPure system (Barnstead/Thermolyne Corp., Boston, MA, USA). All sample solutions were prepared by serial dilution of stock solutions with DDW and acidified to 1% v/v with high purity (sub-boiled, distilled) HNO_3 or HCl. The solutions were stored in pre-cleaned, high-density polyethylene bottles. Head space gas above samples of liquid mercury (ACS grade, BDH, Toronto, ON, Canada) and iodine crystals (analytical reagent, AnalaR, BDH Chemicals, Toronto, ON, Canada) was introduced into the source to permit study of steady-state signals.

General procedures

Mass spectrometry data were collected using steady-state (continuous) and transient furnace temperature programs. Data files were exported from the Elan signal graphics program for subsequent numerical evaluation (*i.e.*, peak area) using in-house software. Where possible, at least two isotopes of a given element, a proximate background mass and a potential oxide ion mass (M + 16), were monitored using a peak hopping routine. Gas flows supplied to the work-head were calibrated using a bubble flow meter. In all cases, a slight overpressure was used to reduce the diffusion of atmospheric gases into the source and the possibility of plasma quenching.

Volatile analyte sample introduction. For steady-state sample introduction, the plasma was initiated and a stable temperature was established before data acquisition. The furnace was operated at ≈500 °C for all measurements, a temperature close to the estimated gas kinetic temperature of a 100 W plasma.[4] A fixed flow rate of He was passed through a sealed 2 mL sample vial containing either $Hg_{(l)}$ or $I_{2(s)}$. The volatile component was mixed with the plasma gas supply prior to entering the work-head. For the experiments described below, Ar was added to the He plasma gas upstream of the point where the Hg or I_2 flux entered. The concentration of the volatile analyte in this mixture was thus diluted in proportion to the ratio of the gas volume flowing through the sample vial to that delivered to the work-head. Using this method of sample introduction, analyte travels through the plasma volume primarily by entrainment within flow profiles that develop upstream of the sampling orifice and pass through the furnace. As a result, only a portion of the gas introduced into the work-head enters the plasma volume. A more efficient, direct sample introduction method for gas effluents has earlier been described by Jimenez and Sturgeon[19] and successfully utilised by Sturgeon and Guevremont[8] with MS detection.

The vapour pressure of mercury at 295 K is 1.88×10^{-8} atm.[15] If it is assumed that the He (250 mL min^{-1}) passing over a bead of metallic Hg becomes saturated with the atomic vapour, then a flux of 3.2×10^{-10} mol s^{-1} Hg will be supplied to the work-head at room temperature. Given that the volume of the ICC is 50-fold smaller than the volume of the work-head and that a homogeneous mixture exists within the work-head, then $\approx 6.4 \times 10^{-12}$ mol s^{-1} Hg (1.3 ng s^{-1}) actually enters the plasma volume. Similarly, the vapour pressure of iodine at 295 K is 3.88×10^{-4} atm.[12] Assuming that the He (90 mL min^{-1}) passing over a crystal of I_2 becomes saturated with I_2 vapour, then a flux of 2.4×10^{-8} mol s^{-1} I_2 will enter the work-head at room temperature. For comparison, atomization of 10 pg of Pb within a 1s period gives rise to a flux of approximately 5×10^{-14} moles s^{-1} Pb. In both cases, the total analyte vapour load is significantly less (trace) than that of the He plasma gas (≈4 mmol s^{-1}). For both analytes, the system is first optimised using a pure He plasma to provide a good general set of conditions for the sampling and transfer of analyte ions through the interface. It is subsequently fine tuned for other mixtures.

Discrete liquid sample introduction. The work-head has a port directly above the furnace injection hole to permit introduction of aqueous samples with the use of an adjustable microlitre pipette. Signal transients from analytes were recorded using the following procedure. A 10 μL sample volume of test solution was pipetted into the ICC furnace and dried by applying a thermal program consisting of a 10 s ramp to 100 °C followed by a hold for 20 s. The residue was then "ashed" at 300 °C or 500 °C by applying a 10 s ramp and 20 s hold. The ash temperature selected was based on a consideration of the volatility of the element in order to prevent sample loss. During the "ashing" cycle, the plasma was initiated by applying the rf power (100 W, 0 W reflected) and data acquisition was then manually triggered approximately 5 s prior to the atomisation event. Automatic impedance matching was not permitted during the heating cycles and, as such, the reflected power would momentarily reach values greater than 25 W for an atomisation temperature of 2300 °C. After each run, a high temperature cycle (2500 °C, 3 s) was initiated and a fixed period of time (60 s) elapsed before the next sampling in an effort to eliminate contamination and ensure consistency in the thermal program for all samples.

Results and discussion

General properties of Ar–He mixed gas system

Although a number of publications focus on the sampling and gas dynamics of Ar (*cf.* refs. 20–22) and He plasma (*cf.* refs. 23–26) systems, few, if any, complementary discussions of the sampling of Ar–He mixed gas systems in plasma mass spectrometry are available. As such, there is merit in reviewing some basic properties of Ar–He mixed gases, especially when considering the low temperature environment of the current system. Table 2 lists some general physical properties of He and Ar.

Source effects. There are a number of effects that occur in the work-head when the gas composition is changed from pure He to mixed Ar–He plasmas. In general, as the Ar gas content is increased, the gas temperature increases and the stability of the plasma visually appears to decrease. The central electrode develops a much deeper red colour arising from heating due to energetic collisions with the larger Ar gas atoms. These unstable, high temperature conditions reduce the lifetime of the ICC tube and electrode through accelerated erosion.

As indicated in Table 2, the thermal conductivity of the gas decreases with increasing Ar content. As such, the gas flow is less efficient at removing heat from the system, resulting in a higher tube temperature. The higher wall temperature of the

Table 2 Select physical properties of the He and Ar plasma gases

Property	He	Ar
Mass/amu	4	40
Mass/kg	6.64×10^{-27}	6.64×10^{-26}
First ionization potential/eV[a]	24.48	15.76
Thermal conductivity/mW mK^{-1} [a]		
300 K	150	17.7
800 K	307	37.0
C_p/C_v[b] (γ)	1.67	1.67
Diameter/Å[c]	2.58	3.42
Collisional cross section/$Å^2$ [c]	21	36

[a]Taken from ref. 14. [b]Ratio of the specific heat capacities of the gas at constant pressure (C_p) and volume (C_v). [c]Taken from ref. 27.

furnace increases the potential for loss of more volatile analyte sample components. These effects have been observed for medium/high volatility elements such as Pb and Bi, where losses during the ashing cycle can be severe if the temperature is not reduced when using gas mixtures containing Ar.

Increasing the Ar gas content within the work-head alters the gas flow profiles. Fig. 1a is a plot of the relative volume of pure He and pure Ar that flows through the 0.5 mm diameter sampling orifice as a function of gas temperature per unit time. These data were calculated using the physical properties of the gases (Table 2) and the gas dynamic equations discussed by Douglas and co-workers.[20,21] At a typical steady-state furnace temperature of 500 °C, approximately four-fold as much He is drawn through the sampler per unit time than Ar and, as the relative Ar concentration increases in mixtures, the amount of He drawn through the sampler decreases (described in more detail further below).

Changes in the gas flow rate through the orifice will subsequently alter the gas flow profiles upstream of the orifice. The theoretical gas velocity for both He and Ar at a position 5 mm upstream of the sampling orifice was calculated[20,21] assuming a stagnant source and plotted in Fig. 1b as a function of gas temperature. This position corresponds to the typical tube–orifice separation distance and thus represents the gap over which diffusion occurs prior to sampling. From the velocity plots in Fig. 1b, the approximate time it takes for a He or Ar gas atom to travel from the end of the furnace to the sampling orifice can be calculated by summing the velocities averaged over small distance increments. These values are indicated in Fig. 1b. Assuming that the analyte achieves bulk flow velocity of the gas, there is a significant difference in the time required for the analyte to travel from the tube to the sampler when pure He is used as compared to pure Ar. This time differential is a function of gas composition, the exact relationship being unknown but crudely estimated using the following approximations. The relative flow velocities of the gas mixtures listed in Table 3 are bounded by the two pure gas values and, because both He and Ar are monatomic ideal gases, the γ value given in Table 2 will remain constant, regardless of composition. Therefore, the calculated[20,21] velocity of the gas mixture will be proportional to the average atomic mass of the mixture. At the maximum concentration of Ar ($\approx$ 9% v/v) used in this study, the average atomic mass is 7.3 g mole^{-1}, which increases the total transport time from 1.5 ms in pure He to 2 ms in such a mixture. Given that the diffusion coefficients for mid-mass elements such as Ba are of the order of 0.5 cm^2 s^{-1} in pure He at 800 K,[28] diffusion based losses over these distances are probably not severe. At 15 mm from the sampling orifice, which corresponds to the centre point of the ICC tube, the calculated transport times are 40, 53 and 124 ms for 0%, 10% and 100% Ar, respectively, at 500 °C. At 25 mm, which corresponds to the distant (back) end of the tube, the transport times are calculated to be 181, 245 and 572 ms, respectively. The total transit-time, and hence the residence time of an analyte, increases with Ar gas content. Longer residence times of the analyte within the plasma volume may improve its ionisation efficiency. It should be stressed that these calculations are meant only to demonstrate that, based upon first principles, there will be a relative decrease in the centre line gas velocities as a function of increasing Ar content. They by no means account for any additional flow profiles generated from the natural flow of gas into the work-head. It is expected, however, that under steady-state conditions, flow profiles will develop that are strongly influenced by such gas entrainment.

Interface effects. As the gas mixture flows into the sampling orifice, it transforms to a continuum free jet expansion. The centre line of the isentropic region (zone of silence) of the expansion is sampled 4.5 mm downstream by a skimmer (X_o = 4.5 mm). For monatomic 'ideal' gases (γ = 5/3), the free jet centre line properties (*i.e.*, temperature, number density and collision frequency) will behave in a similar manner, although their absolute values will be determined largely by the atomic mass of the gas.[29] As such, the relative centre line number density for Ar, He, or Ar–He mixtures will decrease in similar ways. The results are calculated and presented in Fig. 2a using the gas dynamic equations described in the literature.[20-22,29]

In practice, a number of events may occur within the first vacuum stage that can alter the composition of a gas mixture. Collectively these are known as 'separation effects'[30–34] and although they are most prominent in gas mixtures having large mass disparity amongst the components, they can also influence the relative isotopic composition of an element or species detected downstream. As a gas mixture expands into the

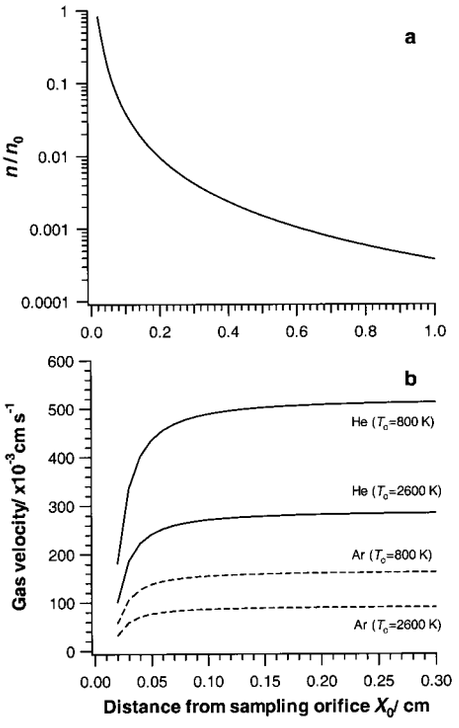

Fig. 2 Gas flow parameters for He and Ar downstream of the 0.5 mm diameter sampling orifice (low pressure). **a** Change in source number density as a function of distance downstream from the sampler for a monatomic ideal gas (γ = 5/3). **b** Change in gas velocity as a function of location downstream of the sampler, calculated using source temperatures of 800 K and 2600 K.

Table 3 Relative composition of the He–Ar mixed gas delivered to the FAPIMS work-head at 298 K and 1 atmosphere

Relative flow rate/L min^{-1}		Gas composition (% v/v) per minute		Gas composition (% w/w) per minute			
He	Ar	He	Ar	He	Ar	Mass flux/ g min^{-1}	Average atomic mass/ g mol^{-1}
4.95	0.00	100.00	0.00	100.00	0.00	0.80	4.0
4.95	0.10	98.02	1.98	83.19	16.81	0.97	4.7
4.95	0.20	96.12	3.88	71.22	28.78	1.13	5.4
4.95	0.30	94.29	5.71	62.26	37.74	1.29	6.1
4.95	0.50	90.83	9.17	49.75	50.25	1.62	7.3

low-pressure region, a diffusive separation can occur in which an enrichment of the heavier component along the centre line results. As described by Sherman[31] and demonstrated by Rothe,[32] this effect is primarily restricted to regions in the under expanded portion at, or immediately downstream of, the sampling orifice where appreciable number density exists. The separation effect is reduced substantially as the gas undergoes a transition to free molecular flow and both species assume directed collisionless flow. Examination of Fig. 2a indicates that the terminal velocity for pure He and Ar gas expansions at source temperatures of $T_o = 800$ and 2600 K is achieved at distances less than 2 mm from the orifice (or $X_o/D < 4$). Skimming of the centreline flow at $X_o = 4.5$ mm results in the transmission of a molecular beam that is enriched in the greater mass component. For the experiments reported here, the greater relative concentration of Ar along the centre line upstream of the skimmer may subsequently affect the acceleration and focusing of analyte species entrained in the expansion in a manner different from that for pure He. In the transport of neutral beam species past the skimmer, off-axis components present in the trajectory of lighter gases will result in their preferential loss and a greater enrichment of heavier species along the centre line.

As a caveat, there are two additional separation effects that may significantly affect the composition of the beam. The diffusion of background gases into the isentropic expansion can result in significant modification of the mixed gas beam composition ratio, primarily favouring the lighter component.[34] As well, the placement or location of the skimmer can significantly affect the composition of the beam which is efficiently transmitted into the second stage.[30] To avoid large deviations, the skimming should be performed well within the Mach disk. For pure He, the Mach disk location can be calculated to occur at $X_M = 5.33$ mm and 9.24 mm behind the sampler orifice for source temperatures of $T_o = 800$ and 2600 K, respectively [using $X_M = 0.67D(P_o/P_b)^{1/2}$].[29] The tip of the skimmer is currently located at $X_o = 4.5$ mm, well upstream of the Mach disk. Further considerations (not explicitly discussed) that may affect the beam composition and background pressure (P_b) in the first stage are non-homogeneous sampling of the mixture and differences in the pumping efficiency of light and heavy gases within the MS.

Velocity slip is another effect that should be considered. Simply put, velocity slip is the difference in the mean velocities of different species. The data plotted in Fig. 2b show the terminal velocity limits for He (light) and Ar (heavy) expansions. For the Ar–He mixtures used in the experiments reported here (Table 3), Ar will be preferentially accelerated towards the terminal velocity of He, obtaining a greater kinetic energy than that normally achieved in pure Ar. Often, however, the heavier component will fail to achieve the terminal velocity of the carrier gas, resulting in velocity slip. Miller has estimated that only a 2% velocity slip occurs for a 3% Ar–97% He mixture at 300 K.[29] Takahashi *et al.*[35] have also demonstrated that differences are further enhanced with larger mass ratios.

Although velocity slip can result in bimodal velocity distributions within an Ar–He gas mixture where the mass ratio is 10 : 1, it will be even more severe for larger mass ratios, such as those encountered with analytes such as Hg ($\approx$50 : 1) and I_2 ($\approx$65 : 1). Of particular relevance to the work described here has been the use of I_2 as an optical marker used to seed various expansion gases so that the flow profiles can be imaged using fluorescence techniques (*e.g.*, refs. 36 and 37). Notably, it is often the case that when I_2 is seeded ($<0.1\%$) in He it does not generate the expected expansion profile, most likely due to the large mass ratio and diffusion separation. For the measurement of Hg and I_2 species reported here, it is therefore likely that these species do not achieve the terminal velocity of the carrier gas and that there will be a relative concentration enhancement along the centre line. The addition of Ar might serve to accelerate these large species through an increased collision frequency (based on hard-sphere collision cross sections) achieving more efficient transfer of energy. This would result in a greater probability of the heavy mass analyte attaining the velocity maximum determined by the He carrier. A mathematical treatment of the I_2–He system by Chidiac *et al.*[38] has confirmed a large velocity slip. Similar experiments in Ar (mass ratio $\approx$5 : 1) show the expected flow profiles, indicating that I_2 more closely approaches the flow characteristics of Ar (*e.g.*, ref. 36). The relative composition of a gas mixture will therefore determine the relative degree of velocity slip and therefore relative differences in the ion kinetic energies and hence ion-optic focussing voltages for different ions.

Impact of mixed gas plasmas on vacuum requirements. When mixed gas Ar–He plasmas are employed, vacuum requirements are reduced. The relative reduction is dependent on the composition of the gas mixture and can be approximated using the aforementioned gas dynamic equations.[20,21] For example, if it is estimated that the gas temperature at the sampling plate located 5 mm downstream of the source is 500 K, then approximately 4.80 L min^{-1} of He will be drawn through the sampling orifice. This flow rate would result in a theoretical pressure in the first stage of $\approx$3.5 Torr, consistent with that measured experimentally. Under normal operation the work-head is usually supplied with 105% of this value, or 5.0 L min^{-1}, to minimise atmospheric ingress. Similarly, it is calculated that, for pure Ar, 1.6 L min^{-1} is drawn through the sampling orifice at 500 K giving an interface pressure of 1.1 Torr. For a mixture containing 0.1 L min^{-1} Ar, Ar accounts for $\approx$6.6% of the gas drawn through the orifice (assuming homogeneous sampling) and therefore only 98.4% of the 5.0 L min^{-1} He balance, or 4.7 L min^{-1} He will be drawn through the sampler. When the mixture contains 0.5 L min^{-1} Ar, it accounts for $\approx$33% of the gas drawn through the orifice and therefore only 3.45 L min^{-1} of the He balance flows through the orifice. For gas mixtures containing 0.0, 0.1, 0.2, 0.3, 0.5 L min^{-1} Ar with 5.0 L min^{-1} He the corresponding interface pressures, read from a pirani gauge (calibrated for air), are 3.8, 3.1, 2.6, 2.3 and 1.7 Torr, respectively.

The crude method described above indicates that, even with the addition of 0.5 L min^{-1} Ar, 3.5 L min^{-1} He is still drawn through the sampling orifice, implying that a significant pumping capacity will still be required. Decreasing the sampling orifice diameter may reduce the vacuum requirements but this usually diminishes the analyte transport efficiency into the MS. As such, although the use of mixed Ar–He plasmas reduces vacuum requirements, they are not large enough to permit the use of significantly smaller pumps.

Constant flux sample introduction

The effect of Ar on Hg^+ and I_2^+ signal intensity. A constant flux of Hg (3.2×10^{-10} mol s^{-1}, 64 ng s^{-1}) is introduced into the FAPIMS work-head gas supply at room temperature. A portion flows through the ionising region of the source (100 W, 500 °C) prior to entering the MS. For a constant He plasma gas flow rate of 4.95 L min^{-1}, an increase in Ar content from 0 to 0.5 L min^{-1} results in a 10-fold increase in the total Hg^+ signal intensity, as shown in Table 4. For each gas mixture, the single lens element (ring lens) was optimised to generate the maximum signal intensity for $^{202}Hg^+$.

The net $^{202}Hg^+$ signal intensities reported in Table 4 are influenced by a number of factors. By increasing the Ar content in the gas mixture, a more energetic plasma[9,10] having increased electron density, ionisation temperature and gas kinetic temperature is generated. The general decrease in the HgO^+/Hg^+ ratio is consistent with this. Also, longer residence times associated with increased Ar content (discussed above) will probably improve the ionisation efficiency. Changes in the gas

Table 4 The effect of Ar content on the Hg^+ MS signal intensity[a]

Ar gas flow rate/L min^{-1}	$^{202}Hg^+$/counts s^{-1}	$^{202}Hg^{16}O^+/^{202}Hg^+$ (%)
0.00	1.76×10^5	3.94
0.10	1.86×10^6	0.38
0.20	1.73×10^6	0.29
0.30	1.87×10^6	0.19
0.50	1.85×10^6	0.18

[a]100 W, He gas flow rate of 4.95 L min^{-1}.

density arising from an increase in source temperature, however, may adversely affect the response through a volume dilution effect. Within the expansion, changes in the overall velocity slip (Hg^+ kinetic energy) are expected in the beam. Optimisation of the lens element should help correct for this and any changes due to variation in source temperatures. In general, only a small increase in the Ar gas content ($\approx$2% v/v) is necessary to generate a significant increase in signal intensity for Hg^+.

A flux of 2.4×10^{-8} mol s^{-1} I_2 was similarly introduced into the plasma gas supply at room temperature. Under steady-state conditions, two major ions (I^+, *m*/*z* 127; I_2^+, *m*/*z* 254) and one minor ion (1–5%, $I_2(H_2O)^+$, *m*/*z* 272) were detected. For simplicity, only the signal intensity for each major ion is listed in Table 5. Fig. 3 shows a plot of the summed signal intensity for all three iodine species arising for each mixture and normalised to that recorded in pure He. A net signal enhancement occurs with increasing Ar content. In each case, the single lens element (ring lens) was optimised to generate the maximum signal intensity for each species and those optimum values summed. Similar to the Hg^+ response, only a small addition ($\approx$2% v/v) of Ar is necessary to generate a significant increase in the total iodine signal intensity.

Data presented in Table 5 indicate that, as the Ar content is increased, there is a shift from the diatomic form to the monatomic form of iodine. The I_2^+/I^+ ratio decreases by over 100-fold for the gas compositions studied. The ionisation potentials for I^+ and I_2^+ are given in Table 1 and the dissociation energies *D*(I-I) and *D*(I-I^+) are 1.54 eV and 2.72 eV, respectively.[39] It is conceivable that the more *energetic* Ar containing plasmas [*e.g.*, increased analyte ionisation temperature (5270 K to 6740 K), electron number density (*i.e.*, He 8×10^{13} cm^{-3}, Ar 1×10^{15} cm^{-3}) and gas kinetic temperature] are more efficient in dissociating the molecular iodine, generating a greater population (2 : 1) of atomic iodine for ionisation. An increase in the collision induced dissociation (CID) of the molecular species in the expansion due to the presence of an acceleration potential and the greater collision frequency that may be experienced with Ar due to its larger cross-section (Table 2) may also contribute to the increased fragmentation. Irrespective of whether dissociation occurs within the plasma (from I_2 or I_2^+) or in the expansion region (from I_2^+), the addition of Ar generates a net signal enhancement for the sum of the iodine species and especially for I^+. The data in Table 5 indicate that there is a significant enhancement (10 : 1) in the atomic ion intensity (I^+) whereas there is only a slight increase (<2 : 1) in the molecular ion (I_2^+)

Table 5 Effect of Ar content on iodine MS signal intensity[a]

Ar gas flow rate/L min^{-1}	$^{127}I^+$/ counts s^{-1}	$^{254}I_2^+$/ counts s^{-1}	$^{254}I_2^+/^{127}I^+$
0.00	1.63×10^4	1.53×10^5	11.00
0.10	1.58×10^6	2.77×10^5	0.18
0.20	9.47×10^5	1.11×10^5	0.13
0.30	8.47×10^5	7.47×10^4	0.09
0.50	7.85×10^5	4.79×10^4	0.06

[a]100 W, He gas flow rate of 4.95 L min^{-1}.

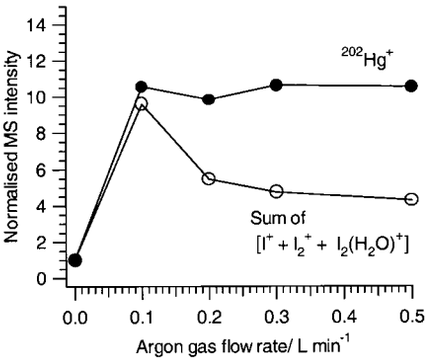

Fig. 3 Signal intensities recorded for $^{202}Hg^+$ and the sum of the major iodine species [$^+$, *m*/*z* 127; I_2^+, *m*/*z* 254, $I_2(H_2O)^+$, *m*/*z* 272] as a function of gas composition. Argon is added to a 100 W plasma (500 °C) supplied by a constant helium gas flow rate of 4.95 L min^{-1}. All signals are normalised to that from the pure He plasma.

intensity. While an in-depth correlation of the Grotrian diagrams for the atomic and molecular forms of iodine with those of Ar and He may provide additional pertinent information it is beyond the scope of the present work.

An interesting observation made during the optimisation procedure for I_2 is that the focusing potential on the single lens element increases with *decreasing* analyte mass. This is illustrated by the data given in Fig. 4a for 4% Ar–96% He mixture at 500 °C. Although the resolution (1 V) is too large to properly define the optimum, the asymmetry in the peak shapes of the plots indicate a smaller difference between the high mass species [*e.g.*, I_2^+–$I_2(H_2O)^+$] than between the high mass–low mass species (*e.g.*, I_2^+–I^+). Under normal Ar ICP-MS operation, the lens potential increases with mass.[40] A possible explanation for this phenomenon might arise from differences in the velocity slip experienced for I^+ and I_2^+ species for which the I^+ : He mass ratio is only half of that of the I_2^+ : He ratio. As such, the lighter analyte may have a greater probability of achieving the terminal velocity of the expansion gas and, therefore, a higher kinetic energy. To account for these observations however, differences in the square of the velocity for the I^+ species must be greater than two times that of the I_2^+. A second, and perhaps more important contribution, may arise from differences in the (hard sphere) collision cross-sections between I^+ and I_2^+ and, consequently, their collisional frequency in regions of significant background gas density. In the presence of an accelerating field, the smaller ion will achieve a greater velocity and a larger relative kinetic energy due to fewer *retarding* collisions. This is qualitatively analogous to classical ion mobility experiments where smaller ions tend to have greater mobility in a given field. This of course presumes that significant ion–electron charge separation has occurred in the ionised gas prior to sampling.

The effect of Ar content on the optimum lens voltage setting for I^+ is shown in Fig. 4b. There is a general increase in the lens voltage required to achieve the optimum signal intensity with increasing Ar content. This is consistent with higher source temperatures. It is also consistent (albeit arguably) with a reduction in velocity slip and closer attainment of the terminal velocity of the He bath gas.

Discrete sample introduction

Signal transients generated using mixed gas plasmas. The effect of increased Ar content on the transient signals generated from 10 pg Pb was investigated. Results are summarized in Table 6 and reflect the average of 5 replicates. In all cases, Ar gas (0.0–0.5 L min^{-1}) is added to a fixed (optimum) He gas flow rate (5.1 L min^{-1}). The lens voltage was optimized for each set of measurement conditions and only small adjustments were required between mixtures.

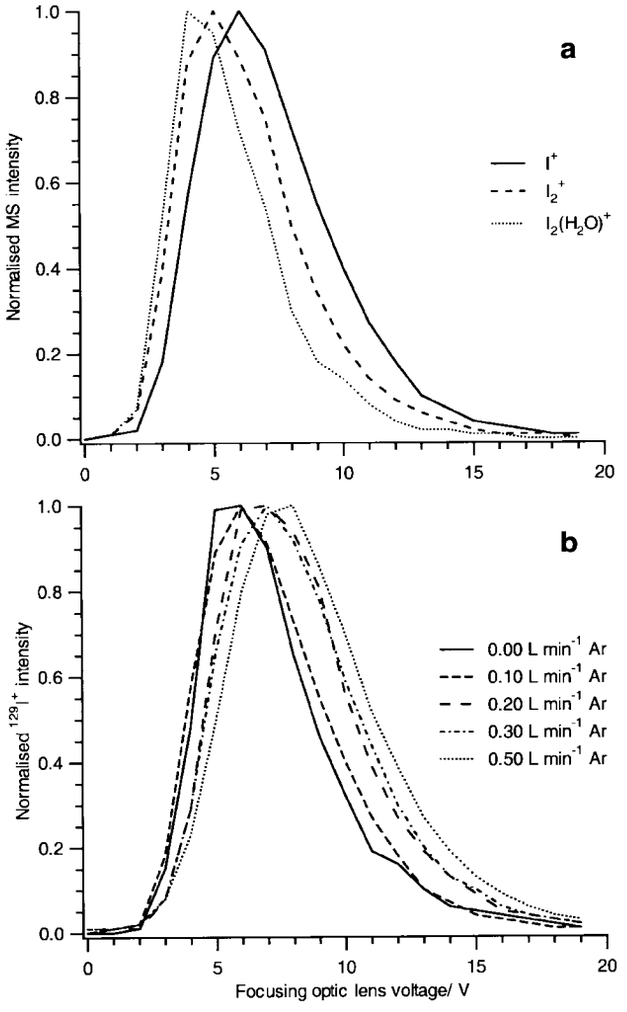

Fig. 4 Effect of the ring lens ion optic focusing voltage on steady-state analyte signal intensity acquired with a 100 W plasma at an ICC temperature of 500 °C. **a** Relative response for iodine plasma species at a gas composition of 4.95 L min^{-1} He and 0.10 L min^{-1} Ar. **b** Relative response of the $^{127}I^+$ ion as a function of argon gas content (Table 3) at a fixed He gas flow rate of 4.95 L min^{-1}.

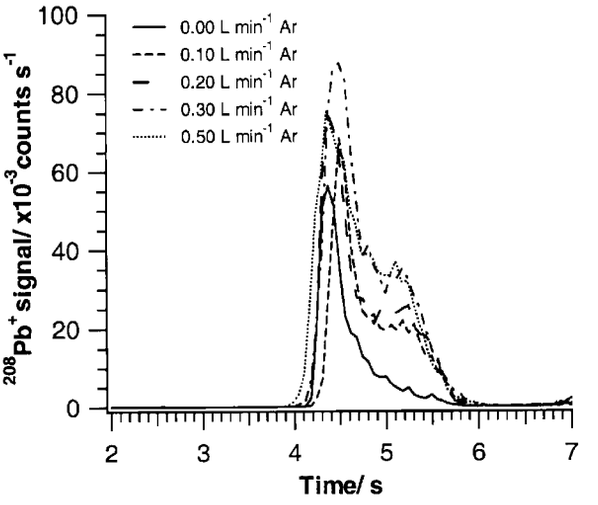

Fig. 5 $^{208}Pb^+$ transients obtained for the atomisation (2300 °C) of 10 pg of Pb in 1% HNO_3 as a function of gas composition (Table 3). The plasma power was 100 W and the He gas flow rate was fixed at 5.1 L min^{-1}. Some relevant statistics are given in Table 6.

Fig. 5 shows typical $^{208}Pb^+$ signal transients recorded for the five different gas mixtures. With reference to Table 6, the data indicates that the addition of Ar leads to an increase in the $^{208}Pb^+$ MS signal for all measurement conditions. From the signal profiles, it appears that the presence of only a small amount of Ar is necessary to increase the $^{208}Pb^+$ MS signal intensity, with the effect accruing most noticeably in the later stages of the transient evolution. Also, a slight shift to earlier appearance times occurs for the $^{208}Pb^+$ transient with increasing Ar content (0.1–0.5 L min^{-1}). This is consistent with higher tube temperatures for a given heating program (as discussed earlier).

It is difficult to compare the signals recorded in Ar directly with those obtained in pure He because the ash temperatures which define the heating ramp were slightly different. The selection of different ash temperatures was necessary in order to maximize the signal while minimizing sample loss due to uncontrolled volatilization during this step. These problems were most significant for the more volatile elements such as Pb and Bi. For less volatile elements, small variations in the optimum ash temperature were not problematic. Nevertheless, it is important to note that the gas composition can influence the efficiency of the atomizer and therefore should be considered when making comparisons of signal intensity. A further indication of the elevated source temperature experienced with Ar content is given by the noticeable decrease in PbO^+/Pb^+ ratio. Addition of Ar appears to generate a higher temperature, more energetic plasma capable of dissociating the oxide.

Analytical figures of merit. Table 7 lists the relative enhancement factors, estimated limits of detection and metal oxide ratios obtained for the analytes listed in Table 1. The elements selected cover a wide range of ionisation potentials and volatility. The enhancement factor is defined as the ratio of the integrated peak area measured for a given analyte in a 4% Ar–96% He plasma to that recorded in a 100% He plasma. Transient signals were recorded for at least two isotopes where possible so that the identity of the signal detected could be easily confirmed if the correct isotope ratios were obtained.

Enhancements were observed for most of the elements studied. A plot of the relative enhancement factor for each element *versus* the first ionisation potential is given in Fig. 6. The enhancement factors for Hg^+ and I^+–I_2^+ are also included for completeness. The enhancement factor appears to correlate with ionisation potential where the smallest (negative) enhancement arises from the alkali metals and the greatest from Pt, I_2 and Hg. In general, there is a slight

Table 6 The effect of Ar content on $^{208}Pb^+$ MS figures of merit[a]

Ar/L min^{-1}	Peak area/counts	Enhancement factor[b]	LOD[c]/fg	Precision[d](%)	PbO^+/Pb^+ (%)
0.00	22597	1.00	5	5.6	3.72
0.10	36652	1.62	8	5.4	0.56
0.20	47391	2.10	4	5.3	0.37
0.30	59508	2.63	8	5.0	0.35
0.50	63939	2.83	6	5.0	0.32

[a]Calculated from 10 pg Pb in 1% HNO_3, using a plasma power of 100 W and a He gas flow rate of 5.1 L min^{-1}. [b]The enhancement factor is expressed as the ratio of the integrated area of the analyte obtained in Ar–He mixture to that obtained in pure He. [c]Limit of detection (LOD) calculated as 3× the standard deviation of the blank based upon 10 replicates. [d]Based on five replicate measurements.

Table 7 Effect of argon gas content on analyte limits of detection (LOD), enhancement factors and metal oxide ratio[a]

Analyte	Ar flow rate/L min^{-1}	Detection limit[b]/fg	Enhancement factor[c] (M^+_{Ar} area/M^+_{He} area)	MO^+/M^+ (%)
^{56}Fe	0.00	200		2.0%
	0.20	N.A.	N.A.	N.A.
^{85}Rb	0.00	46		<0.1
	0.20	14	0.50	<0.1
^{108}Pd[d]	0.00	2000		<0.1
	0.20	1600	3.60	<0.1
^{113}In	0.00	90		<0.1
	0.20	20	1.03	<0.1
^{133}Cs	0.00	40		<0.1
	0.20	10	0.75	<0.1
^{174}Yb[d]	0.00	4000		26.0
	0.20	2000	1.83	2.0
^{195}Pt[d]	0.00	70000		10.0
	0.20	10000	4.24	1.2
^{208}Pb	0.00	5		3.72
	0.20	4	2.10	0.40
^{208}Bi	0.00	28		4.0
	0.20	17	3.80	2.0

[a]Calculated from signal transient (10 pg) peak areas and a 1% (v/v) HNO_3 blank. Plasma power: 100 W, He plasma gas flow rate: 5.1 L min^{-1}. [b]Limit of detection (LOD) calculated as 3× the standard deviation of the blank based upon 10 replicates. [c]The enhancement factor is expressed as the ratio of the integrated area of the analyte obtained in Ar–He mixture to that obtained in pure He. [d]Analyte mass of 1 ng was used.

improvement in the estimated detection limits calculated from the Ar–He mixed gas plasmas relative to the pure He plasma with the largest effect obtained for Pt. Excluding Pt, which has the highest ionisation potential, the detection limits for most elements are in the ppt to sub-ppt range based upon a 10 μL sample volume. The presence of Ar did not significantly increase the background for most of the elements studied. The data in Table 6 suggest that, with the gas compositions used, the precision of the measurement may even improve with Ar. Therefore, the decrease in detection limits is due primarily to an increase in the signal intensity for the elements studied. It is anticipated that the detection limits for many of these elements could reach the ppq range with further optimisation of the sampling conditions and interface.

Ionisation mechanism in the Ar–He mixed gas plasma

The data in Fig. 6 indicate that the enhancement factor increases as a function of ionisation potential for the elements studied. It has earlier been concluded[6] that, for a 50 W He plasma, elements with first ionisation potentials (IP) below 6 eV are 100% ionised whereas those around 9 eV may only be 5% ionised. For a 100 W He plasma, the ionisation efficiency is expected to increase, particularly for those elements having the highest IP. For comparison, in an Ar ICP, the ionisation efficiency may be as high as 70% for elements with IP ⩽ 9 eV,[41] which is 14-fold greater than that obtained in He FAPES plasma.

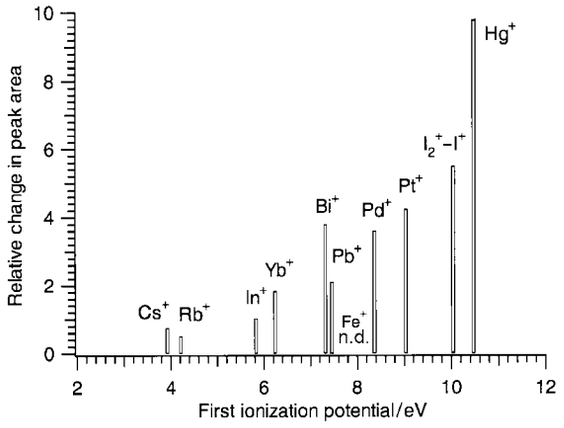

Fig. 6 Relative signal enhancement for various elements as a function of their first ionisation potential. All enhancements are calculated from the ratio of the integrated transient peak areas acquired in the Ar (0.2 L min^{-1})–He (5.1 L min^{-1}) mixture to that in the pure He plasma (100 W, 5.1 L min^{-1}).

The addition of Ar to the plasma gas supply should therefore increase the degree of ionisation for elements having an IP greater than 6 eV. This trend is observed in Fig. 6; elements such as the alkali metals and In do not show significant enhancements whereas Pt, I_2 and Hg, which have the greatest IP, show the most significant enhancements. At this point, it is unclear whether the slight decrease in signal for Cs^+ and Rb^+ is a result of plasma processes or differences in transmission efficiency that may occur with the addition of Ar. Although the data generated from the selected elements indicate that the increase in ionisation efficiency occurs largely through the associated increase in electron density, ionisation temperature and gas kinetic temperature, it does not preclude the impact of other mechanisms such as charge transfer or Penning ionisation.[9,10]

The effect of Ar on the spectral background

The background signal intensity recorded in the pure He FAPIMS source has been previously discussed by Stewart *et al.*[2] In general, background species originate from gas supply contaminants, atmospheric gases entrained into the work-head, surface contamination within the work-head and gas supply lines, and carbonaceous species. The last are especially prevalent at a high source temperature. Although entrainment can be minimised by supplying an overpressure of plasma gas to the work-head, and surface contamination can be minimised through high temperature 'cleaning' cycles, both are difficult to completely eliminate. The addition of Ar under low temperature furnace operation (*e.g.*, 500 °C) generally leads to an increase in only the $^{40}Ar^+$ signal, which is roughly proportional to the added Ar flow rate. During atomisation (*e.g.*, 2300 °C) other species such as ArC^+, ArO^+ and Ar_2^+ become quite intense and, as such, degrade the detection power for elements having the same nominal mass (*i.e.*, $^{52}Cr^+$, $^{56}Fe^+$ and $^{80}Se^+$). In this respect, Ar–He mixed gas plasmas suffer background problems similar to those encountered with Ar-ICP-MS.

Formation of MO^+ and M^{2+} ions

The data given in Tables 4, 6 and 7 suggest that the addition of Ar reduces the relative metal-oxide signal intensity. In most cases, an approximately 10-fold reduction is achieved with the addition of 0.2 L min^{-1} Ar. As illustrated by the Pb data given in Table 5, a minimum is reached with no further reduction in the PbO^+/Pb^+ ratio for Ar content above 0.2 L min^{-1} Ar. The reduction in the metal oxide ratio through the addition of Ar to the plasma gas is most likely the result of the efficient atomisation associated with a more energetic plasma.

Ytterbium was included in this study as an example of a low volatility element with an atomisation temperature (2500 °C)[14] that is not too high to significantly impede its ionisation in the FAPIMS source due to high reflected powers caused by the emission of electrons from the heated tube walls.[42] Ytterbium is also prone to oxide formation where $D_{Yb\text{-}O}=4.12$ eV and $D_{Yb\pm O}=3.82$ eV.[43] The data in Table 7 indicate a substantial presence of oxide, which is subsequently reduced in the presence of Ar. Despite the relatively low second IP of Yb (12.1 eV), no conclusive evidence for the presence of Yb^{2+} was detected, nor was there any evidence for the second ionisation of any of the other elements studied (Table 1). Although Ba is often used as a marker element for the formation of M^{2+} ions in plasmas due to its relatively low second IP, its atomisation temperature (≈2700 °C) is too high for useful determinations with FAPIMS and therefore it was not tested.

Conclusions

A major impact of the addition of Ar to the He gas supply in the FAPIMS source appears to be the generation of more 'energetic' plasmas which have greater electron density, higher ionisation temperatures and gas kinetic temperatures. This explains, in part, the correlation between the signal enhancements observed for an element and its ionisation potential. Elements with ionisation potentials below 6 eV that are presumed 100% ionised produce no signal enhancements, whereas those with greater IP exhibit enhancements which increase with IP. Additional element specific mechanisms, such as charge transfer reactions and Penning ionisation, may also occur. Further support for this is the enhanced dissociation of molecular species such as I_2^+ and YbO^+, having dissociation energies between 2 and 4 eV. This presumably occurs due to more efficient atomisation of molecular species within the plasma and suggests that the addition of Ar might be a useful tool for the fragmentation of other organic or organometallic species enabling the attainment of elemental information or structural information.

Mixed Ar–He gas plasmas should be used with caution. The addition of Ar can reduce the thermal conductivity and increase the furnace wall temperature, leading to inadvertent loss of volatile components if measures are not taken to reduce the ashing temperature. Also, the different gas compositions will influence the flow velocity of analyte into the sampling orifice and hence transport and/or residence times within the plasma volume. The nature of the impact of mixed gas plasmas downstream of the sampler remains unclear. Although the beam composition and, hence, energetics of the expansion may change with gas composition, the effects do not appear to dramatically limit or enhance the determination of the elements studied.

Only a small concentration (≈10%) of Ar is required to generate significant analyte signal enhancements whereas larger amounts result in an unstable plasma and a high temperature environment which contributes to significant erosion of the graphite tube and electrode surfaces. The small amount of Ar used does not significantly ease the pumping requirements on the interface. The development of different gas introduction arrangements, sampling or interface designs may, however, generate more efficient sampling conditions. For example, by contouring the sampling orifice to better entrain the gas flowing from the source the orifice diameter requirements may be reduced and hence the pumping capacity. Such investigations are presently underway in this laboratory.

Acknowledgements

The authors wish to thank Scott D. Tanner and PE-SCIEX for the ELAN 6000 testbed mass spectrometer used in this study. The technical assistance of Peter L'Abbe is also greatly appreciated.

References

1 R. E. Sturgeon and R. Guevremont, *Anal. Chem.*, 1997, **69**, 2129.
2 I. I. Stewart, R. Guevremont and R. E. Sturgeon, *Anal. Chem.*, 1999, **71**, 5146.
3 W. Frech, D. C. Baxter and B. Hutsch, *Anal. Chem.*, 1986, **58**, 1973.
4 S. Imai and R. E. Sturgeon, *J. Anal. At. Spectrom.*, 1994, **9**, 493.
5 D. C. Gregoire and R. E. Sturgeon, *Spectrochim. Acta, Part B*, 1999, **54**, 773.
6 R. E. Sturgeon and R. Guevremont, *J. Anal. At. Spectrom.*, 1998, **13**, 229.
7 A. Montaser, S-K. Chan and D. W. Koppenaal, *Anal. Chem.*, 1987, **59**, 1240.
8 R. Guevremont and R. E. Sturgeon, *J. Anal. At. Spectrom.*, 2000, **15**, 37.
9 F. Sun and R. E. Sturgeon, *J. Anal. At. Spectrom.*, 1999, **14**, 901.
10 F. Sun and R. E. Sturgeon, *Spectrochim. Acta, Part B*, 1999, **54**, 2121.
11 R. E. Sturgeon, S. N. Willie, V. T. Luong, S. S Berman and J. G. Dunn, *J. Anal. At. Spectrom.*, 1989, **4**, 669.
12 R. E. Sturgeon, S. N. Willie, V. T. Luong and S. S Berman, *Anal. Chem.*, 1990, **62**, 2370.
13 T. D. Hettipathirana and M. W. Blades, *Spectrochim. Acta, Part B*, 1992, **47**, 493.
14 W. Slavin, *Graphite Furnace AAS – A Source Book*, The Perkin-Elmer Corporation Spectroscopy Division, Ridgefield, CT, USA, 1984, pp. 18–19.
15 *CRC Handbook of Chemistry and Physics*, ed. R. C. Weast and M. J. Astle, CRC Press Inc., West Palm Beach, Fl, 1978, 59th edn.
16 *Ionization Potential and Appearance Potential Measurements, 1971–1981*, NSRDS-NBS 71, ed. R. D. Levin and S. G. Lias, US Government Printing Office, Washington, D.C., 1983.
17 C. W. Le Blanc and M. W. Blades, *Spectrochim. Acta, Part B*, 1995, **50**, 1395.
18 R. E. Sturgeon, V. Pavski and C. L. Chakrabarti, *Spectrochim. Acta, Part B*, 1996, **51**, 999.
19 M. S. Jiminez and R. E. Sturgeon, *J. Anal. At. Spectrom.*, 1997, **12**, 597.
20 D. J. Douglas and J. B. French, *J. Anal. At. Spectrom.*, 1988, **3**, 743.
21 D. J. Douglas and S. D. Tanner, in *Inductively Coupled Plasma Mass Spectrometry*, ed. A. Montaser, Wiley-VCH, New York, 1998, ch. 8, pp. 615–679.
22 H. Niu and R. S. Houk, *Spectrochim. Acta Part B*, 1996, **51**, 779.
23 D. W. Koppenaal and L. F. Quinton, *J. Anal. At. Spectrom.*, 1988, **3**, 667.
24 D. M. Chambers, J. W. Carnahan, Q. Jin and G. M. Hieftje, *Spectrochim. Acta Part B*, 1991, **46**, 1745.
25 H. Zhang, S-H. Nam, M. Cai and A. Montaser, *Appl. Spectrosc.*, 1996, **4**, 427.
26 A. Montaser and H. Zhang, in *Inductively Coupled Plasma Mass Spectrometry*, ed. A. Montaser, Wiley-VCH, New York, 1998, ch. 10, pp. 809–890.
27 P. W. Atkins, *Physical Chemistry*, W.H Freeman and Co., New York, USA. 1986, 3rd edn.
28 R. K. Namiotka, E. Ehrlacher, J. Sagle, M. Brewer, D. J. Namiotka, A. P. Hickman, A. D. Streater and J. Huennekens, *Phys. Rev. A*, 1996, **54**, 449.
29 D. R. Miller, in *Atomic and Molecular Beam Methods*, ed. J. Scolas, Oxford University Press, Oxford, 1988, vol. 1.
30 V. H. Reis and J. B. Fenn, *J. Chem. Phys.*, 1963, **39**, 3240.
31 F. S. Sherman, *Phys. Fluids*, 1965, **8**, 773.
32 D. E. Rothe, *Phys. Fluids*, 1966, **9**, 1643.
33 N. Abuaf, J. B. Anderson, R. P. Andres, J. B. Fenn and

D. R. Miller, *Rarefied Gas Dynamics-Proceedings of the 5th International Symposium*, 1967, pp. 1317–1336.
34 R. Campargue, *J. Chem. Phys.*, 1970, **52**, 1795.
35 N. Takahashi, T. Moriya and K. Teshima, *Rarefied Gas Dynamics-Proceedings of the 13th International Symposium*, 1985, pp. 939–950.
36 K. Teshima and H. Nakatsuji, *Rarefied Gas Dynamics-Proceedings of the 14th International Symposium*, 1984, pp. 447–454.
37 A. Fujimoto, S. Kato, M. Usami, T. Niimi and and S. Kamiya, *Rarefied Gas Dynamics-Proceedings of the 14th International Symposium*, , 1984, pp. 467–475.
38 C. Chidiac, M. Y. Perrin and J. P. Martin, *Phys. Fluids A*, 1991, **3**, 1991.
39 A. G. Gaydon, *Dissociation Energies and Spectra of Diatomic Molecules*, Chapman and Hall Ltd., London, 1968, 3rd edn.
40 E. R. Denoyer, D. Jacques, E. Debrah and S. D. Tanner, *At. Spectrosc.*, 1995, **16**, 1.
41 R. S. Houk, *Anal. Chem.*, 1986, **58**, 97A–105A.
42 R. E. Sturgeon, V. T. Luong, S. N. Willie and R. K. Marcus, *Spectrochim. Acta, Part B*, 1993, **48**, 893.
43 E. Murad and D. L. Hilderbrand, *J. Chem. Phys.*, 1980, **73**, 4005.